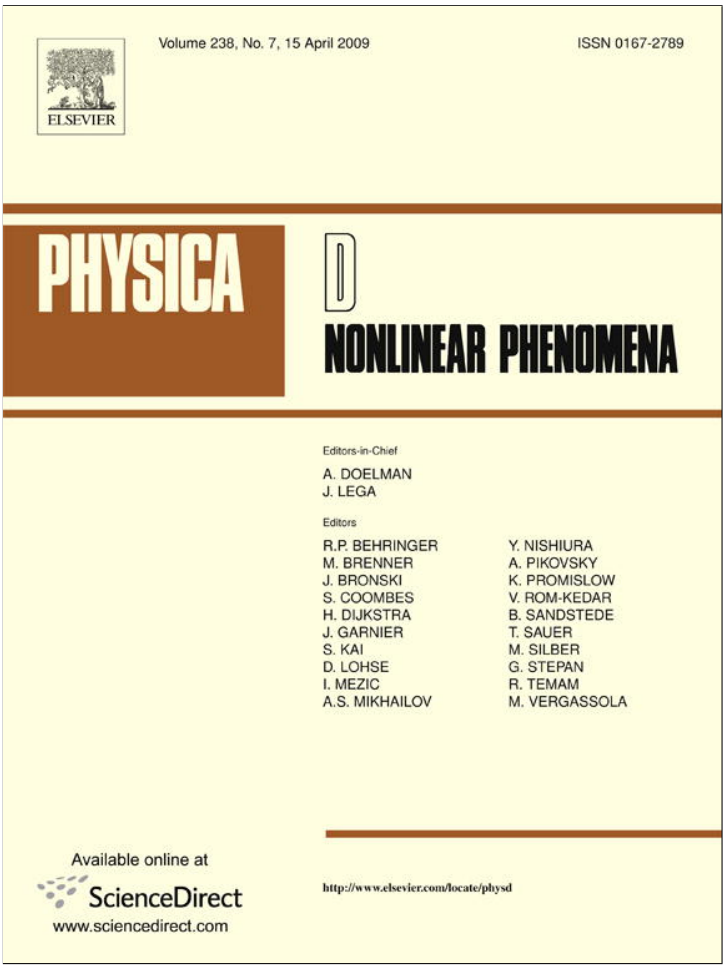

Physica D 238 (2009) 771–781

Contents lists available at ScienceDirect

Physica D

journal homepage: www.elsevier.com/locate/physd

Synchrony due to parametric averaging in neurons coupled by a shared signal

Anmar Khadra *

Institute for Theoretical Biology, Humboldt University of Berlin, Invalidenstraße 43, 10115 Berlin, Germany

ARTICLE INFO

Article history:
Received 9 May 2008
Received in revised form
12 January 2009
Accepted 18 January 2009
Available online 30 January 2009
Communicated by V. Rom-Kedar

PACS:
87.10.+e

Keywords:
GnRH neurons
Synchrony
Reduction
Common pool
Phase
Averaged model

ABSTRACT

Gonadotropin-releasing hormone (GnRH) is a decapeptide secreted by GnRH neurons located in the hypothalamus. It is responsible for the onset of puberty and the regulation of hormone release from the pituitary. There is a strong evidence suggesting that GnRH exerts an autocrine regulation on its own release via three types of G-proteins [L.Z. Krsmanovic, N. Mores, C.E. Navarro, K.K. Arora, K.J. Catt, An agonist-induced switch in G protein coupling of the gonadotropin-releasing hormone receptor regulates pulsatile neuropeptide secretion, Proc. Natl. Acad. Sci. 100 (2003) 2969–2974]. A mathematical model based on this proposed mechanism has been developed and extended to explain the synchrony observed in GnRH neurons by incorporating the idea of a common pool of GnRH [A. Khadra, Y.X. Li, A model for the pulsatile secretion of gonadotropin-releasing hormone from synchronized hypothalamic neurons, Biophys. J. 91 (2006) 74–83]. This type of coupling led to a very robust synchrony between these neurons. We aim in this paper to reduce the one cell model to a two-variable model using quasi-steady state (QSS) analysis, to further examine its dynamics analytically and geometrically. The concept of synchrony of a heterogeneous population will be clearly defined and established for certain cases, while, for the general case, two different types of phases are introduced to gain more insight on how the model behaves. Bifurcation diagrams for certain parameters in the one cell model are also shown to explain some of the phenomena observed in a coupled population. A comparison between the population model and an averaged two-variable model is also conducted.

1. Introduction

Hormonal regulation of mammalian reproduction occurs at three different levels. The gonadotropin-releasing hormone (GnRH), secreted by synchronized GnRH neurons in the hypothalamus, is at the highest level of this hierarchical control [2]. It is carried by the local blood circulation to the pituitary where it triggers the release of two intermediate hormones, the luteinizing hormone (LH) and the follicle-stimulating hormone (FSH), from gland cells called the gonadotrophs. LH and FSH are carried by the general circulation to the local glands, ovaries in females and testis in males, where they stimulate the release of estrogen and testosterone, respectively. It has been found that the temporal profile of the GnRH signal is quite critical for maintaining a normal secretory activity of the gonadotrophs. This signal must be pulsatile [2–4], i.e., sharp pulses separated by intervals of near-zero baseline levels, with a frequency which is specific to different species [5]. In primates, including humans, for example, it is about one pulse per hour. A constant GnRH signal or a pulsatile one with the "wrong" frequency suppress the secretory activities of the gonadotrophs. Furthermore, the GnRH signals with the "correct" temporal profile artificially introduced to immature monkeys are capable of inducing precocious maturation and sexual development [6]. These results demonstrate that the pulsatile GnRH signal is both necessary and sufficient for mammalian reproduction. As a matter of fact, the absence of this signal leads to a number of reproductive diseases such as sterility. Therefore, understanding the mechanisms underlying the origin of this signal is of great clinical and fundamental value.

It is now believed that GnRH secretion is an intrinsic property of GnRH neurons [7–10] and that only a few thousands of these sparsely distributed neurons are involved in this pulse generator [11]. Given this relatively small number, synchronization is presumed to play a central role in the GnRH rhythmogenesis. Although the mechanism underlying this synchrony remains largely unknown, it has been suggested that a diffusible mediator between these neurons is needed to achieve synchronization [12], while synaptic and gap-junctional coupling between them are not essential [13,14]. Recent experimental evidence reveals that these neurons express receptors for GnRH [14–16], suggesting that this hormone exerts an autocrine regulation on its own release and acts as a synchronizing agent between these neurons [17–19]. For sustained oscillations to occur a positive feedback mechanism must be combined with a negative one to bring the peak values of the pulses back to their basal levels. This can be accomplished by the inhibition of GnRH release by high level of GnRH through a G-protein coupled process [1]. This new evidence, combined with the previous findings of the stimulatory effect of the autocrine regulation,

* Tel.: +49 (0)30 2093 6044; fax: +49 (0)30 2093 8801.
E-mail addresses: khadraan@staff.hu-berlin.de, anmar.khadra@gmail.com.

0167-2789/$ – see front matter © 2009 Elsevier B.V. All rights reserved.
doi:10.1016/j.physd.2009.01.009

seems to form a complete mechanism that explains the origin of pulsatile GnRH release.

We have built in [20] a model describing the dynamics of one neuron based on this mechanism. We showed that this GnRH-regulated GnRH-release mechanism is sufficient for generating pulsatile GnRH release. We have also established that the synchronization of a heterogeneous population of these model neurons mediated by a common pool of diffusible GnRH was very robust. The properties of this model, such as parametric-averaging, recruitment and the minimum fraction of active neurons required to maintain a pulsatile population, were examined in [21].

It should be mentioned here that the coupling technique (common pool) used in [20,21] to generate networks of GnRH model neurons differ considerably from those discussed in other papers. As a matter of fact, the huge literature that exists on phase synchrony of oscillatory networks, including periodic and chaotic models, has been mainly concerned with weak versus strong diffusive coupling (e.g., see [22,23]), and with mean field coupling (e.g., see [24]). The presence of synchronization phenomenon in many biological and engineering problems has induced this extensive work in this field. To mention a few, phase synchrony was analyzed in genetic networks (repressilators) [24], in brain rhythms (such as gamma and beta rhythms) [25], in neurons (e.g., to study clustering) [26], etc. It was also investigated under the influence of noise [27], and in association with chaotic systems [28] for engineering purposes.

Our aim in this paper is to further examine this new coupling technique (which cannot be labeled as weak or strong) by considering the models presented in [20,21]. We intend to nondimensionalize the six-variable model describing the dynamics of one GnRH neuron and reduce it to a two-variable model using quasi-steady state (QSS) approximation. We shall show that this reduced model is bounded and use nullcline analysis to establish many of the stability results stated in [21]. The synchrony between these model neurons coupled by a shared signal (or a common pool) will be shown to be stable for certain types of heterogeneity in the population. As for the general case of a completely heterogeneous population of model neurons, we introduce two different phases, one is based on polar coordinates while the other is based on the notion of Hilbert Transform [29]. They describe the dynamics of the model in a manner similar to the one used in [22]. We finally compare the dynamics of the whole population of model neurons to an averaged two-variable model whose parameters satisfy certain averaging properties and show that this new averaged model could approximate the population model quite adequately.

This paper is organized as follows: In Section 2, we reintroduce the full model presented in [20] and nondimensionalize it to validate the QSS approximation used in Section 3, aimed at reducing the full model to a two-variable model. The reduced model is then analyzed in Section 4, while the notion of synchronization of a population of N-coupled model neurons by a shared signal is discussed in Section 5. In Section 6, a comparison between the dynamics of the population model with an averaged two-variable model is performed. Finally, in Appendix, some concluding remarks are stated.

2. Full model

The pulsatile release of GnRH is an intrinsic property of each GnRH cell. This hypothesis is supported by a number of experiments and is consistent with all known facts. For example, *in vivo* experiments has demonstrated that pulsatility remains intact when the medial basal hypothalamus is surgically disconnected from other parts of the brain. The observation of pulsatile GnRH release from GnRH cells in cultures and the discovery of GnRH receptors in GnRH cells in slices as well as in cultures suggested that GnRH cells can alone generate pulsatile GnRH release without inputs from other cells through an autofeedback mechanism. Additional results suggest also that GnRH acts as a diffusible mediator and as a synchronizing agent.

We have developed in [20] a mathematical model for the GnRH secretion based on this autocrine regulation using a mechanism proposed by Krsmanovic et al. in [1]. The model applied to two cases equally: (a) a large number of identical GnRH cells in a continuously-stirred perfusion chamber; (b) a single GnRH cell located in a small liquid droplet with a volume only slightly bigger than the cell. Case (a) represented a realistic description of experimental perfusion cultures, while case (b) was only a prediction of the model since both cases would lead to identical mathematical equations. The autocrine effect of GnRH on GnRH cells through GnRH receptors played a central role in the formulation of this model, while direct synaptic and gap-junctional coupling were completely ignored for the lack of experimental evidence.

Sequential activation of three types of G-proteins due to GnRH binding to its receptors formed the foundation of the mechanism used in this model (for further details, see [20,21,1]). In other words, it was supposed that the binding of extracellular GnRH (denoted by G) to its receptors on GnRH neurons, could induce dose-dependent activation of three types of G-proteins G_s, G_q and G_i. The activated α subunits of G_s and G_i, denoted by α_s and α_i, were found to dissociate from the membrane and their respective $\beta\gamma$ subunits in order to exert excitatory and inhibitory influences, respectively, on the production of cAMP by adenylyl cyclase (AC). The activated α subunits of G_q, denoted by α_q, was found to activate the production of IP_3 which could trigger Ca^{2+}release from intracellular stores. The dose-dependence of the cytosolic concentration of each activated α subunit on extracellular GnRH concentration (G) was assumed sigmoidal in the model with a Hill coefficient larger or equal to 2. The value of G required for 50% saturation was taken to be small for α_s, medium for α_q and very large for α_i. Furthermore, based on experimental data, the model expressed the dose-dependence of cytosolic Ca^{2+}concentration (C) on G in sigmoid curve, whereas the dose-dependence of cytosolic cAMP concentration (A) on G was expressed in biphasic curve (both at steady state). Many studies showed that intracellular $Ca^{2+}$and cAMP were the two intracellular messegers directly involved in the episodic release of GnRH. Therefore, the model assumed that they work together in triggering GnRH release from GnRH cells in a nonlinear fashion (through a cubic term).

In this model, G played the roles of a diffusible mediator as well as a synchronizing agent. α_s led to a modest increase in the secretion of G through a positive feedback loop (via cAMP) while α_q provided a second positive feedback loop that essentially triggered a sharp increase in the secretion of G (via Ca^{2+}). α_i, on the other hand, provided a slow negative feedback loop which terminated the spike (by inhibiting cAMP production) and kept G at basal level for an extended period during the interspike intervals (of approximately 1 h in primates).

Thus the full model of GnRH pulse generation described in [20] consisted of six variables: G, C, A, S, Q and I, where S, Q and I represented the concentrations of α_s, α_q and α_i, respectively. The dimensioned form of the full model is given in Appendix A. The dimensionless form of this model is given by

$$\frac{dg}{d\tau} = \lambda\left[\nu + \eta(ca)^3 - g\right] \tag{1}$$

$$\frac{dc}{d\tau} = \zeta\left[j_{in} + [\mu + \delta q](c_0 - c) - c\right] \tag{2}$$

$$\frac{da}{d\tau} = \xi\left[\iota + \theta s\frac{\omega}{\omega + i} - a\right] \tag{3}$$

Table 1
Values of the dimensionless parameters of the model given by system (1)–(6).

Symbol	Value	Symbol	Value	Symbol	Value	Symbol	Value	Symbol	Value
λ	0.067	ν	0.706	η	3.292	ζ	566.67	j_{in}	9.227×10^{-6}
μ	0.012	δ	0.588	c_0	0.588	ξ	6.67	ι	1
θ	216.67	ω	0.01125	ϕ	1	σ	1	ψ	1
ρ	61.765	ϵ	0.0125	κ	464.706				

$$\frac{ds}{d\tau} = \phi\left[\frac{g^4}{\sigma^4 + g^4} - s\right] \tag{4}$$

$$\frac{dq}{d\tau} = \psi\left[\frac{g^2}{\rho^2 + g^2} - q\right] \tag{5}$$

$$\frac{di}{d\tau} = \epsilon\left[\frac{g^2}{\kappa^2 + g^2} - i\right], \tag{6}$$

where g, c, a, s, q and i are the dimensionless form of the original variables G, C, A, S, Q and I, respectively (see Appendix A). The scaled parameters ι, ϕ and σ satisfy $\iota = \phi = \sigma = 1$, which will no longer be the case in a heterogeneous population of coupled model neurons. In Table 1, we show the values of all the dimensionless parameters appearing in system (1)–(6). The substitutions used in this nondimensionalization were chosen very carefully to express the rate of each variable clearly in these equations. It will be quite evident in the next section the importance of this step when model reduction is discussed.

3. Reduced model

It was pointed out in [20] that the variations in the two variables C and A are much faster than the changes in the remaining variables, a fact consistent with experimental observations. In fact, when fitting the experimental data available on the steady states of C and A to Eqs. (A.2) and (A.3), the rates of these equations were 2 orders of magnitude faster than the remaining equations. That was the motivation in [20,21] to reduce the six-variable model (1)–(6) to a four-variable model.

We verify this claim here by comparing the values of the two parameters ξ and ζ with those of the parameters λ, ϕ, ψ and ϵ (the former set of parameters are 1-2 orders of magnitude larger than the latter set). Interestingly, the set of parameters ζ, ξ, ϕ and ψ are 2-4 orders of magnitude larger than the parameters λ and ϵ (see Table 1). In other words, the model predicts, through this scaling process, that not only calcium and cAMP dynamics are fast, but also the two distinct positive feedback loops exerted by the two subunits α_s and α_q are significantly faster than the negative feedback loop exerted by α_i (a common feature among other biological systems). This suggests that the model consists of two subsystems: (i) a fast one consisting of the variables c, a, s and q; (ii) slow one consisting of the variables g and i.

The variable i represents an essential element for the oscillations to occur in this model (see [20,21]). It expresses the inhibition exerted by α_i on the GnRH hormone to bring the pulse back to its basal level. In the absence of inhibition, GnRH pulsatility disappears and gets replaced by an elevated steady state. Such behaviour can be demonstrated by setting the variables g and i equal to constants (due to their slow-varying behaviour) and solving for the fast subsystem. In Appendix B, we show that the solution of each variable in the fast subsystem, except for c, is expressed explicitly in terms of constant terms and exponential functions with negative powers. As for c, we also show that this variable can be expressed asymptotically in the same way. In other words, the fast subsystem is a nonoscillatory system and converges quickly to its steady state (as predicted intuitively). The rate of convergence, in this case, is determined by the large rate constants ζ, ξ, ϕ and ψ which happened to be the very same parameters used initially to divide the full model into two subsystems. The nondimensionalization used in Appendix A was therefore quite essential to identify the two subsystems within the full model.

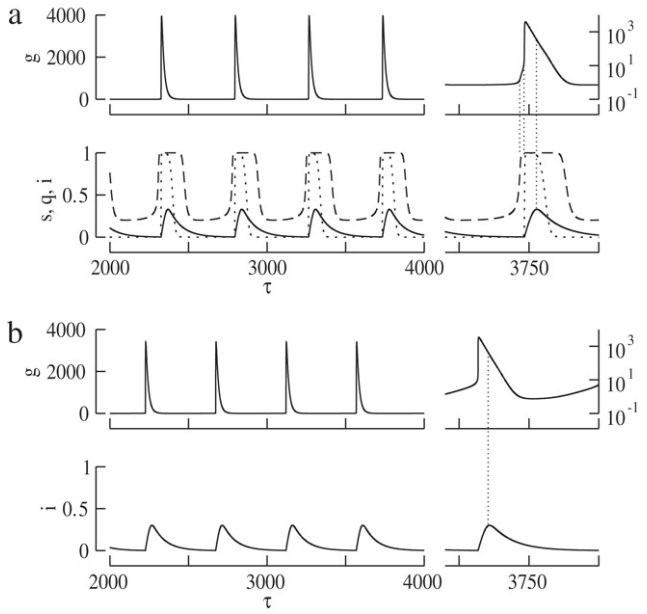

Fig. 1. Numerical simulation of (a) the full model (1)–(6), and (b) the reduced model (7) and (8). The profile of g (solid line) is shown in the upper panels, while the profiles of s (dashed line), q (dotted line) and i (solid line) are shown in the lower panels. The left panels show the direct action of each subunit on g (plotted in logarithmic scale).

The above analysis suggests that the oscillations generated by the full model will not be affected by setting the fast subsystem to its steady state. Therefore, we can reduce the full model to a two-variable model by applying QSS approximation on the variables c, a, s and q to obtain

$$\frac{dg}{d\tau} = \lambda\left[\nu + \eta F(g, i) - g\right] \tag{7}$$

$$\frac{di}{d\tau} = \epsilon\left[H(g) - i\right], \tag{8}$$

where $F(g, i) = [c_\infty(q_\infty)a_\infty(s_\infty, i)]^3$, $H(g) = g^2/(\kappa^2 + g^2)$ and

$$c_\infty(q_\infty) = \frac{J_{in} + (\mu + \delta q_\infty)c_0}{\mu + 1 + \delta q_\infty},$$
$$a_\infty(s_\infty, i) = \iota + \theta s_\infty \frac{\omega}{\omega + i} \tag{9}$$
$$s_\infty = \frac{g^4}{\sigma^4 + g^4}, \qquad q_\infty = \frac{g^2}{\rho^2 + g^2}.$$

Fig. 1(a) shows the profiles of g (upper panel) and s, q and i (lower panel) for the full nondimensionalized model while Fig. 1(b) shows the profiles of g (upper panel) and i (lower panel) for the reduced model. They clearly demonstrate that both models exhibit nearly identical behaviours except for very minor differences in their amplitude and frequency, consistent with our previous discussion. When viewing the profile of g in logarithmic scale in panel (b),

we see clearly the level of g initially rising steadily due to s (at steady state), followed by a sharp rise due to q (at steady state) until reaching a threshold that activates the inhibition exerted by i. In other words, g exerts an autocatalytic influence on its own secretion via s_∞ and q_∞, while i exerts negative feedback effect on g, generating oscillations displayed by a pulsatile and episodic manner (see Fig. 1(b)).

4. Analytical results on the reduced model

In this section, we shall analyze analytically and geometrically some of the properties of system (7) and (8). We begin first by showing that the solution trajectories of this system are bounded in the state space.

Proposition 1. *Solution trajectories of system (7) and (8) are bounded (or globally stable).*

Proof. By integrating equation (8) starting at $\tau = \tau_0$, we obtain

$$i(\tau) = \epsilon \int_{\tau_0}^{\tau} \frac{g^2(\overline{\tau})}{\kappa^2 + g^2(\overline{\tau})} \mathrm{e}^{-\epsilon(\tau-\overline{\tau})} \mathrm{d}\overline{\tau}.$$

But $0 \le g^2(\overline{\tau})/(\kappa^2 + g^2(\overline{\tau})) \le 1$, for all $\overline{\tau} \in [\tau_0, \tau]$. This implies that $0 \le i(\tau) \le 1 - \exp[-\epsilon(\tau - \tau_0)] < 1$, for all $\tau \in [\tau_0, +\infty)$. Similarly, by integrating equation (7), we obtain

$$g(\tau) = \lambda \int_{\tau_0}^{\tau} [\nu + \eta F(g(\overline{\tau}), i(\overline{\tau}))] \mathrm{e}^{-\lambda(\tau-\overline{\tau})} \mathrm{d}\overline{\tau}.$$

From Eq. (9), we may conclude that $0 < s_\infty < 1, 0 < q_\infty < 1$ and

$$0 \le F(g, i) < \left[\frac{j_{in} + (\mu + \delta)c_0}{\mu + 1 + \delta}(\iota + \theta)\right]^3 =: L,$$

for all $\overline{\tau} \in [\tau_0, \tau]$, since $j_{in} - c_0 < 0$ (see Table 1), where L is some positive constant. It follows that $0 \le g(\tau) < \nu + \eta L$, for all $\tau \in [\tau_0, +\infty)$. In other words, the solution trajectories $\mathbf{x}(\tau) = (g(\tau), i(\tau))$ are bounded. □

The latter proposition indicates that the solution trajectories of system (7) and (8) will always approach an attractor in the state space. According to the Poincare–Bendixson Theorem, this attractor could be either (a) a stable equilibrium, (b) a stable limit cycle, or (c) a homoclinic or a heteroclinic orbit. These three cases might even coexist. The i-nullcline associated with system (8) is simply the Hill function $i = H(g)$, but the g-nullcline cannot be expressed explicitly. Fig. 2 shows both nullclines associated with Eqs. (7) and (8) and their point of intersection $(\log(g^*), i^*) = (0.12887, 2.2522)$. This point represents the only equilibrium solution the system possesses. Increasing the parameter κ shifts the i-nullcline to the left, while decreasing the parameter ν shifts the g-nullcline downward and to the right. If the g-nullcline is sufficiently shifted downward, then two additional equilibria will be generated. On the other hand, decreasing the parameters ω, lowers the main peak in Fig. 2(b) while the parameter ϵ does not affect the shape of the i-nullcline which is expected in view of Eq. (8). In other words, varying these four key parameters may allow the system to possess up to three equilibria.

We shall now derive the necessary and sufficient conditions for the equilibrium (g^*, i^*) to be stable. In order to do so, we state the following important inequalities that are inherent properties of system (7) and (8).

$$\frac{\partial F}{\partial g} > 0 \tag{10}$$

$$\frac{\partial F}{\partial i} < 0 \tag{11}$$

$$\frac{\mathrm{d}H}{\mathrm{d}g} > 0. \tag{12}$$

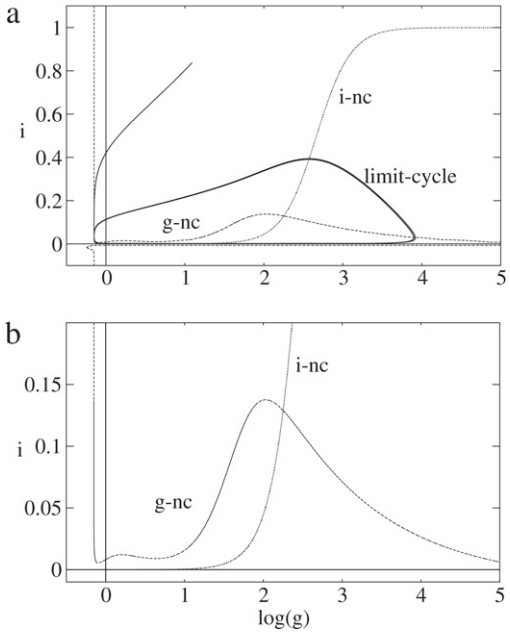

Fig. 2. (a) The i and g-nullclines associated with system (7) and (8) are shown together with a periodic orbit. (b) As in (a) except that the nullclines have been magnified close to their point of intersection. The g-axes (horizontal axes) in both panels follow the logarithmic scale.

Inequality (10) is satisfied because the two subunits α_s and α_q stimulate GnRH secretion, while inequality (11) is satisfied because α_i inhibits GnRH secretion. Since $H(g)$ is a steadily increasing Hill function of g, it follows that (12) is also satisfied. Now we are ready to state the following proposition for arbitrary functions F and H satisfying inequalities (10)–(12).

Proposition 2. *Let D_g and D_i be the slopes of the tangent lines to the g and i-nullclines, respectively. Then any given equilibrium (g^*, i^*) of system (7) and (8) is stable if and only if*

$$D_i > D_g \tag{13}$$

and

$$0 < \frac{\partial F}{\partial g} < \frac{1}{\eta}\left(\frac{\epsilon}{\lambda} + 1\right) \tag{14}$$

are satisfied at (g^*, i^*).

Proof. Recall that the necessary and sufficient conditions for a system consisting of 2 variables to possess a stable equilibrium (x^*, y^*) are: $\det(J) > 0$ and $\mathrm{tr}(J) < 0$ at (x^*, y^*), where $\det(J)$ and $\mathrm{tr}(J)$ are the determinant and trace of the Jacobian matrix of the two-variable system, respectively. Let's now evaluate the Jacobian matrix of system (7) and (8):

$$J = \begin{pmatrix} \lambda\eta\dfrac{\partial F}{\partial g} - \lambda & \lambda\eta\dfrac{\partial F}{\partial i} \\ \epsilon\dfrac{\mathrm{d}H}{\mathrm{d}g} & -\epsilon \end{pmatrix}.$$

Thus

$$\det(J) = \epsilon\lambda\left[\left(1 - \eta\frac{\partial F}{\partial g}\right) - \eta\frac{\partial F}{\partial i}\frac{\mathrm{d}H}{\mathrm{d}g}\right]$$

and

$$\mathrm{tr}(J) = \lambda\left[\eta\frac{\partial F}{\partial g} - 1\right] - \epsilon.$$

Inequalities (10)–(12) imply that the equilibrium (g^*, i^*) is stable whenever

$$\frac{1}{\eta}\left(\frac{1}{|\partial F/\partial i|}\right) + \frac{\mathrm{d}H}{\mathrm{d}g} > \left(\frac{\partial F/\partial g}{|\partial F/\partial i|}\right),$$
$$\frac{\partial F}{\partial g} < \frac{1}{\eta}\left(\frac{\epsilon}{\lambda} + 1\right).$$

Since

$$D_g = \frac{\partial F/\partial g}{|\partial F/\partial i|} - \frac{1}{\eta}\left(\frac{1}{|\partial F/\partial i|}\right) \quad \text{and} \quad D_i = \frac{\mathrm{d}H}{\mathrm{d}g},$$

it follows that inequalities (13) and (14) are the necessary and sufficient conditions for (g^*, i^*) to be stable. □

Remark 1. Inequality (14) is equivalent to

$$0 < \left|\frac{\partial F}{\partial i}\right| < \frac{\epsilon}{\eta\lambda D_g}.$$

Remark 2. If inequality (13) and the equation

$$\frac{\partial F}{\partial g} = \frac{1}{\eta}\left(\frac{\epsilon}{\lambda} + 1\right)$$

are satisfied, then the equilibrium point (g^*, i^*) is a Hopf bifurcation point where two branches of periodic solutions emerge.

Fig. 2(b) clearly demonstrates that the only equilibrium point (g^*, i^*) of system (7) and (8) satisfies inequality (13), because $D_i > 0$ and $D_g < 0$. In fact, decreasing (increasing) the value of the parameter κ moves this equilibrium to the left (right) along the g-nullcline while never violating inequality (13). In other words, (g^*, i^*) could either be a stable or an unstable equilibrium but never a saddle point. This means that system (7) and (8) cannot possess a homoclinic orbit originating from (g^*, i^*). Since the solution trajectories of system (7) and (8) are bounded (Proposition 1), it follows that a stable limit cycle must exist whenever the point (g^*, i^*) is unstable. This occurs when (g^*, i^*) lies on the part of the g-nullcline with positive slope (i.e., when $D_i > D_g > 0$ and inequality (14) is violated). If the equilibrium point (g^*, i^*) is stable, on the other hand, we cannot draw any conclusions about the existence of a stable limit cycle in this case. The phase plane of system (7) and (8), shown in Fig. 2(a), reveals, however, that the point (g^*, i^*) is not globally attractive and that a stable limit cycle coexists with this stable equilibrium. By using XPP, the eigenvalues associated with the point (g^*, i^*), in this case, are given by $-0.026196 \pm \mathrm{i}0.060098$, both of which have negative real parts, so the point (g^*, i^*) is a stable focus.

There are four key parameters that play important roles in determining the general dynamics of the model [21]. These 4 parameters are κ, ω, ϵ and ν. In brief, the parameter κ specifies the threshold level for activating the α_i subunit, ω determines the threshold value of α_i beyond which the production of cAMP is significantly inhibited, ϵ is the time scale of the i variable, while ν is the basal level of GnRH production. The bifurcation diagrams of the variable g with respect to these four parameters are shown in Fig. 3.

For the parameter κ, stable periodic solutions (thin/solid line) could be observed for two different ranges (see Fig. 3(a)). Each range is bounded by two subcritical Hopf bifurcation points at which bistability between a limit cycle and an elevated steady state (thick/solid line) is observed outside the range, while a stable limit cycle surrounding an unstable equilibrium (thick/dashed line) are observed inside. In the regime where bistability is obtained, an unstable limit cycle (thin/dashed line) acts as a separatrix between the stable limit cycle and the stable steady state. Moreover, the amplitude of the stable limit cycle stays roughly the same in each range, although the amplitude of oscillations in the right range

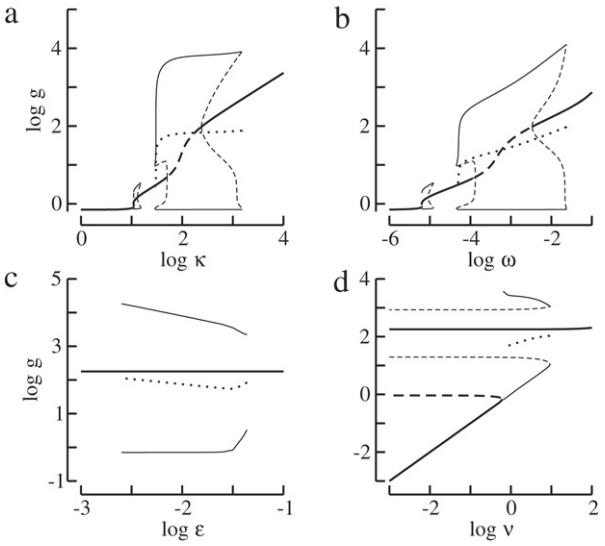

Fig. 3. Bifurcation diagrams of g with respect to 4 key parameters: (a) κ, (b) ω, (c) ϵ and (d) ν. The steady state values of g are plotted in solid (stable) and dashed (unstable) thick lines, whereas periodic solutions are plotted in solid (stable) and dashed (unstable) thin lines in each panel. The dotted thick lines refer to the average of the maximum and minimum values of g along its stable periodic branches. Note that the logarithmic scale is used for all axes and the unstable periodic solutions are not plotted in panel (c).

is significantly larger than those in the left range. It should be mentioned here that for the regime inside the two ranges, the unstable steady state is generated when the i-nullcline, shown in Fig. 2(b), intersects the declining branches of the two peaks of the g-nullcline, as demonstrated in Proposition 2. The presence of the left oscillatory range can explain the reason as to why a population of model neurons coupled together by a shared signal is capable of pulse generation even in the presence of many neurons whose κ-values are low (such behaviour was labeled "recruitment" in [21]).

In the case of the parameter ω, similar type of behaviour is detected (see Fig. 3(b)). Once again, two oscillatory ranges bounded by subcritical Hopf bifurcation points are obtained. The existence of these two ranges reveals that the recruitment phenomenon is expected to occur in this case. The values of the elevated plateau of steady states are also close to those obtained for the parameter κ. The only two noticeable differences in the type of behaviour exhibited by this model in the ω case are: the stable periodic solutions are generated for very small range of values and their amplitude shows sensitive parameter-dependence on ω. The parameter-dependence is expressed by a steady increase in amplitude for increasing values of ω in both ranges. These two differences justify the substantially more robust behaviour exhibited by the population models considered in [20,21] towards heterogeneity with respect to κ than to ω.

As mentioned earlier, the parameter ϵ does not change the shape of the nullclines shown in Fig. 2. Therefore, the coexistence of the stable periodic orbit and the stable/elevated equilibrium, separated by an unstable periodic orbit (not shown), is preserved for a very small range of values of ϵ (see Fig. 3(c)). The smallness of this range accounts for the sensitivity of the population model to heterogeneity in that parameter. The loss of periodic solutions for small ϵ (left end-point of the oscillatory range) is due to the fact that the i variable becomes roughly a constant, eliminating the inhibition exerted by i (a crucial element for pulse generation). This explains why pulsatility disappears in this case. On the other hand, when ϵ is too large (right end-point of the oscillatory range), the pulsatility once again disappears due to fast inhibition, not allowing sufficient amount of g to accumulate for activating i.

As for the parameter ν, many interesting behaviours are exhibited in this case. Fig. 3(d) shows three different regimes in which the global behaviour of system (7) and (8) changes. In the left regime (for small values of ν), two coexisting steady states are observed, one with an elevated level of g while the other one with a near-zero level of g, separated by a saddle point. By increasing ν, the saddle point and the stable steady state with a near-zero level of g merge and disappear, while a branch of stable periodic solutions emerges at a SNIC bifurcation point (saddle-node on invariant circle bifurcation). In this new regime, an unstable periodic orbit acts as a separatrix between the stable periodic orbit and the stable steady state with elevated level of g. Finally, in the right regime (for large ν values), both branches of periodic solutions merge and disappear, leaving behind the only remaining globally stable steady state in the most right regime. It should be mentioned here that the amplitude of the oscillations increases slowly with ν within the oscillatory range, but the size of this oscillatory range is quite large that the robustness of a population model towards parameter heterogeneity in ν is preserved.

We shall see in the next section that the bifurcation diagrams of κ and ν combined will be able to provide some answers as to why periodic injections of exogenous GnRH *in vivo* lead to seemingly contradictory results. It will be shown that the heterogeneity in the population model will generate multistability that is responsible for the apparent inconsistencies in the experimental results.

5. Population model

We have investigated in the previous section the dynamics of a one cell model. Such a model can be extended to describe a whole population of model neurons. Experimental evidence suggests that these neurons are coupled together by a shared signal or a common pool g. It has been observed in [20] that a single model neuron possesses all the necessary parts for generating episodic and pulsatile behaviour, provided that all parameters remain identical across the whole population. In other words, the single-cell model is equivalent to the model of a population of identical model neurons. Obviously, this represents an unrealistic set up, since neurons differ from each other in their natural settings. We aim in this present study to analyze and establish analytically some of these numerical results obtained in [20,21]. We shall first define what we mean by synchrony and establish some synchronization results when limited degree of heterogeneity is considered in the population. We also introduce two different phases that will be helpful in examining the most realistic case when heterogeneity appears in all parameters

A dimensionless form of the model of N heterogeneous GnRH neurons coupled through a common pool of extracellular GnRH is given by the following equations.

$$\frac{\mathrm{d}g}{\mathrm{d}\tau} = \frac{1}{N}\sum_{n=1}^{N}\lambda_n\left[\nu_n + \eta_n F_n(g, i_n) - \frac{\overline{\lambda}_n}{\lambda_n}g\right] \tag{15}$$

$$\frac{\mathrm{d}i_n}{\mathrm{d}\tau} = \epsilon_n\left[H_n(g) - \frac{\overline{\epsilon}_n}{\epsilon_n}i_n\right], \quad (n = 1, 2, \ldots, N), \tag{16}$$

where we use the subscript n in the functions F_n, H_n and the parameters to indicate that they all have different values. We have also assumed here that the ratios $\overline{\lambda}_n/\lambda_n$ and $\overline{\epsilon}_n/\epsilon_n$ are not necessarily equal to 1 for every neuron to emphasize heterogeneity in the degradation terms. The fact that all neurons share a common extracellular concentration of g implies that the extracellular medium is continuously stirred so that GnRH secretion by each neuron is diluted and averaged immediately in the whole medium. This can be regarded as an approximation of the perfusion experiments in which the continuous flow through the chamber can cause a stirring effect. A more realistic model will be considered in a separate study. In the rest of this section, we shall use system (15) and (16) to analyze synchrony in a heterogeneous population of model neurons.

We have introduced in [20,21] a synchrony measure suitable for the model described by system (15) and (16). This synchrony measure used the peaks of the variables i_n, $n = 1, 2, \ldots, N$, to determine if a population of model neurons is synchronized or not. Due to the presence of heterogeneity in the model, the peaks of the i_n variables will never peak at the same moment. A small phase difference will always exist between the peaks of any two variables i_n and i_m, $n, m = 1, 2, \ldots, N$. Therefore, it has been asserted in [20,21] that a population of model neurons are considered "synchronized" if the maximum phase difference between the neurons is smaller than the width of the g-pulse. Notice that the case corresponding to a quiescent population of coupled model neurons in which g is not pulsatile (i.e., all variables are at steady state) is already included in the definition of synchrony. The phase difference in this case could be chosen arbitrarily and the duration of the g-pulse could be chosen to be larger than the maximum phase difference to satisfy the definition. This means that a synchronized population of GnRH neurons could be either quiescent or pulsatile/episodic. From an experimental point of view, the latter behaviour is more interesting than the former, but from a mathematical point of view these two distinct behaviours are inconsequential as far as synchrony is concerned (we shall use this important feature in our later discussion).

Interestingly, our numerical simulations of system (15) and (16) suggest that the quiescent behaviour is due to the inability of the model neurons in the population to maintain both synchrony and pulsatility at the same time. This may explain some of the *in vivo* results obtained [21] when investigating the response of the population model to periodic injections of exogenous g at increasing doses. It has been demonstrated that at a relatively high injection frequency of g (which is equivalent to increasing the value of the parameter ν at each injection), the population model either (i) maintained pulsatility at low and high injection doses, or (ii) became quiescent at intermediate injection doses (i.e., injection doses caused oscillation death in this case). While Fig. 3(d) may explain the outcome obtained for low and intermediate doses, it fails to do so for high doses, as it predicts that for high doses, the population model must remain quiescent. It seems that other factors in the model, such as heterogeneity in the parameters and bistability, are responsible for the this triphasic behaviour. This becomes clear when we consider the bifurcation diagram of κ in Fig. 3(a). Since κ determines the threshold value for activating i in each neuron, injecting g at intermediate doses appears to divide the population model into two subgroups; one subgroup that consists of model neurons with κ values smaller than the dose while the second subgroup consists of model neurons with κ values larger than the dose. Thus when the population model is stimulated by periodic injections of g at intermediate doses, the first subgroup is activated while the second is not. The competition between the two subgroups leads to their dis-synchrony and to oscillation death in the population. For low and intermediate doses, however, one subgroup dominates over the other and episodic and pulsatile g combined with synchrony is preserved. It would be interesting to find out the critical values of the relative sizes of each subgroup at which pulsatility is lost.

Let's now analyze synchrony in system (15) and (16) by first stating the following important result, which is an immediate consequence of Proposition 1.

Corollary 1. *Solution trajectories of system (15) and (16) are bounded (or globally stable).*

It follows that system (15) and (16) must possess at least one attractor in the $(N + 1)$-dimensional space generated by the N coupled model neurons. According to our simulations, however,

the only two attractors generated by this model are steady states and/or limit cycles, both of which imply that synchrony is attained in the population model. This begs the question of what happens to synchrony if the attractor were something else (such as a strange attractor)? Following up on what has been said about synchrony versus the general behaviour of the model, we are able to answer this question analytically for a special case when the heterogeneity in system (15) and (16) persists in all parameters except for $\overline{\epsilon}_n$ and κ_n, i.e., when Eq. (16) is expressed as

$$\frac{di_n}{d\tau} = \epsilon_n \frac{g^2}{\kappa^2 + g^2} - \overline{\epsilon} i_n, \tag{17}$$

where $\overline{\epsilon}_n = \overline{\epsilon}$ and $\kappa_n = \kappa$, for all $n = 1, 2, \ldots, N$. The next proposition shows that the population model described by Eqs. (15) and (17) are synchronized regardless of what type of attractor the model possesses.

Proposition 3. *The population model described by Eqs. (15) and (17) satisfies*

$$\lim_{\tau\to\infty} \frac{i_n}{i_m}(\tau) = \frac{\epsilon_n}{\epsilon_m}$$

for all $n, m = 1, 2, \ldots, N$.

Proof. Let $\Phi_{nm}(\tau) := \tan^{-1}(i_n(\tau)/i_m(\tau))$, $n, m = 1, 2, \ldots, N$ (Φ_{nm} represents the angle in polar coordinates projected onto the $i_n i_m$-plane with $\Phi_{nm} \in (-\pi/2, \pi/2)$). Taking the derivative of Φ_{nm} with respect to τ, we obtain

$$\begin{aligned}
\Phi'_{nm} &= \frac{1}{1 + (i_n/i_m)^2}\left(\frac{i'_n i_m - i'_m i_n}{i_m^2}\right) \\
&= \frac{1}{1 + \tan^2 \Phi_{nm}}\left(\frac{i'_n}{i_m} - \frac{i'_m}{i_m}\frac{i_n}{i_m}\right) \\
&= \cos^2 \Phi_{nm}\left(\frac{i'_n}{i_m} - \frac{i'_m}{i_m}\tan \Phi_{nm}\right).
\end{aligned}$$

But, by Eq. (17), we have

$$\frac{i'_n}{i_m} = \frac{\epsilon_n}{i_m}\frac{g^2}{\kappa^2 + g^2} - \overline{\epsilon}\tan \Phi_{nm}$$

and

$$\frac{i'_m}{i_m} = \frac{\epsilon_m}{i_m}\frac{g^2}{\kappa^2 + g^2} - \overline{\epsilon}.$$

Thus

$$\begin{aligned}
\Phi'_{nm} &= \frac{\epsilon_n}{i_m}\frac{g^2}{\kappa^2 + g^2}\cos^2 \Phi_{nm} - \frac{1}{2}\overline{\epsilon}\sin(2\Phi_{nm}) \\
&\quad - \frac{1}{2}\frac{\epsilon_m}{i_m}\frac{g^2}{\kappa^2 + g^2}\sin(2\Phi_{nm}) + \frac{1}{2}\overline{\epsilon}\sin(2\Phi_{nm}) \\
&= \frac{1}{i_m}\frac{g^2}{\kappa^2 + g^2}\left[\epsilon_n \cos^2 \Phi_{nm} - \frac{1}{2}\epsilon_m \sin(2\Phi_{nm})\right] \\
&= \frac{\cos^2 \Phi_{nm}}{i_m}\frac{g^2}{\kappa^2 + g^2}\left[\epsilon_n - \epsilon_m \tan \Phi_{nm}\right].
\end{aligned}$$

Notice that

$$\frac{\cos^2 \Phi_{nm}}{i_m}\frac{g^2}{\kappa^2 + g^2} > 0 \quad (\text{where } \Phi_{nm} \in (-\pi/2, \pi/2)),$$

so the latter equation possesses only one critical point at $\Phi^*_{nm} = \tan^{-1}(\epsilon_n/\epsilon_m)$. Since $\tan^{-1}(\epsilon_n/\epsilon_m) \in (-\pi/2, \pi/2)$, the one-dimensional phase-portrait of Φ_{nm} implies that Φ^*_{nm} is stable. Thus

$$\begin{aligned}
&\Phi_{nm} \to \Phi^*_{nm} = \tan^{-1}\frac{\epsilon_n}{\epsilon_m} \quad \text{as } \tau \to \infty \\
&\iff \frac{i_n}{i_m} \to \frac{\epsilon_n}{\epsilon_m} \quad \text{as } \tau \to \infty. \quad \square
\end{aligned}$$

It follows from Proposition 3 that after a small transient, each i_n becomes a constant multiple of every other i_m, $n, m = 1, 2, \ldots, N$. This means that regardless of the temporal profile of the i_n variables, the peaks of these variables eventually line up. In the special case when solution trajectories approach an attractive periodic orbit, for example, each one of the i_n variables will exert the inhibition on g simultaneously, leading to a synchronized behaviour. The common pool g, in this case, becomes pulsatile and the i_n variables are periodic with zero-phase difference between them (see [20]). As for other types of attractors, such as steady state (i.e., the quiescent behaviour), quasi-periodic or chaotic attractors, similar conclusions can be reached; the population model will also exhibit perfect phase synchroy between the neurons. The steady state case represents the trivial case analyzed earlier, where each neuron is involuntarily synchronized, while the quasi-periodic and chaotic attractors, the behaviour is identical to the case of an attractive periodic orbit.

When $\epsilon_n = \epsilon$, for all $n = 1, 2, \ldots, N$, in Eq. (17), the synchrony between model neurons in such a population becomes identical, i.e., amplitude and frequency of oscillations become identical across the whole population. This result is summarized in the following proposition.

Proposition 4. *If* $\epsilon_n = \epsilon$ *in Eq. (17), for all* $n = 1, 2, \ldots, N$, *then*

$$\lim_{t\to\infty} |i_n - i_m| = 0,$$

for all $n, m = 1, 2, \ldots, N$.

Proof. Let $\Delta i_{nm} = i_n - i_m$, for some $n, m = 1, 2, \ldots, N$. By taking the derivative of both sides, we obtain

$$\Delta i'_{nm} = i'_n - i'_m = -\epsilon \Delta i_{nm},$$

which implies that $\lim_{t\to\infty} \Delta i_{nm} = 0$, for every n, m. $\square$

As pointed out earlier, in a diversely heterogeneous and pulsatile population of model neurons, in which all parameters differ across the whole population, a small phase difference between the peaks of the i variables will emerge. This makes proving synchrony a much more difficult task. In order to tackle this problem, it would be a good idea to introduce the notion of phase in this case [22]. The proof of Proposition 3 motivates the idea of using the term Φ_{nm} as a possible candidate to quantify the phase difference between two neurons. Briefly, Φ_{nm} describes the phase between i_n and i_m, for $n, m = 1, 2, \ldots, N$, moving along the $(N + 1)$-dimensional solution trajectory of system (15) and (16). Fig. 4(a4) and (b4) show the projections of typical solution trajectories obtained for a system that satisfies the heterogeneity conditions of Proposition 3 and a system whose parameters are all diversely heterogeneous, respectively. By letting

$$\Phi(\tau) = \frac{2}{N(N-1)}\sum_{\substack{n,m=1 \\ n<m}}^{N} \Phi_{nm}(\tau),$$

we could roughly measure the synchronization between the model neurons. For example, according to the heterogeneity conditions stated in Proposition 3, we expect that system (15) and (17) to be fully synchronized since $\Phi \to \pi/4$, as $\tau \to \infty$. Indeed, Fig. 4(a2) shows how Φ approaches this constant level, while in Fig. 4(b2), a periodic Φ with a very small amplitude is generated due to the presence of heterogeneity in all parameters.

Similar type of behaviour could be also observed when we introduce another type of phase based on the notion of Hilbert transform [29]. Hilbert transform of a signal $s(\tau)$ is defined by

$$H(s(\tau)) = \text{p.v.}\int_{-\infty}^{+\infty} \frac{s(\tau - \overline{\tau})}{\pi\overline{\tau}} d\overline{\tau},$$

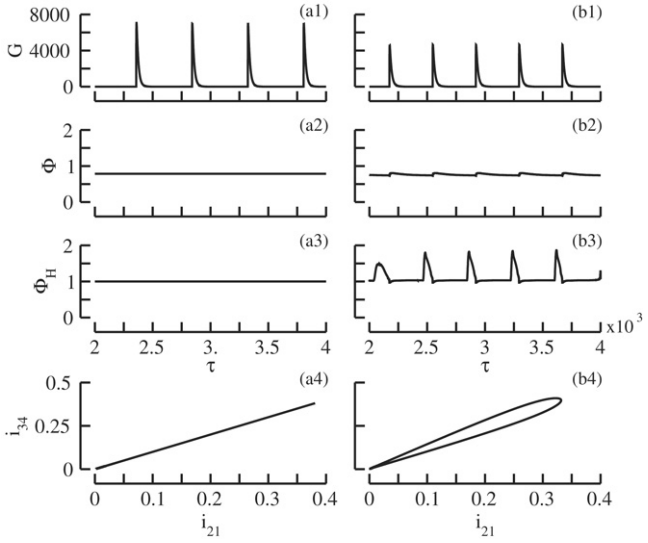

Fig. 4. 50 model neurons coupled together by a shared signal. The left column corresponds to an identical population of GnRH model neurons, while the right column corresponds to a nonidentical population of GnRH neurons possessing heterogeneity in the parameters κ, ω and ϵ. (a1) and (b1) show the simulations of the variable g, (a2) and (b2) show the graphs of the phase Φ, whereas (a3) and (b3) show the graphs of the phase Φ_H obtained from Hilbert transform. Finally, (a4) and (b4) show typical solution trajectories projected onto the $i_{21}i_{34}$-plane. Notice that in the case of identical neurons (a4), the projection is a straight line.

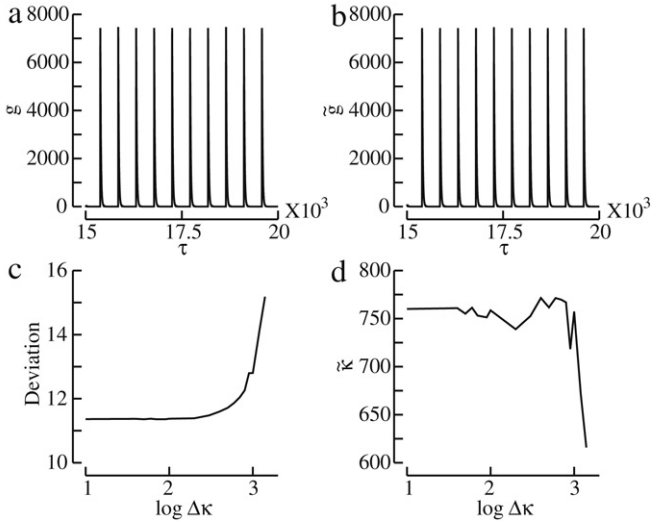

Fig. 5. Comparing the dynamics of the averaged model to that of the population model that possesses heterogeneity in the parameters κ_n only. The temporal profile of g in (a) the averaged model, and (b) the population model, for $\Delta\kappa = 300$, indicate that the frequency and amplitude of g in both cases are almost identical. (c) The deviation measure and (d) the geometric average, $\widetilde{\kappa}$, are both plotted with respect to the length of the range of κ_n.

where p.v. denotes the Cauchy principle value of the integral. Then the phase of the signal $s(\tau)$ is defined by

$$\Phi_H(\tau) = \tan^{-1}\frac{H(s(\tau))}{s(\tau)}.$$

Thus the new phase Φ_H could be evaluated at every variables i_n, $n = 1, 2, \ldots, N$, to determine if such phase exhibits any additional features that could help us understand the dynamics of the general case of a diversely heterogeneous population. Let

$$\Phi_H(\tau) = \frac{2}{N(N-1)}\sum_{\substack{n,m=1\\ n<m}}^{N}\frac{\Phi_{Hn}+U}{\Phi_{Hm}+U}(\tau),$$

where $\Phi_{Hn} = \tan^{-1}H(i_n(\tau))/i_n(\tau)$ and $U > |\min_{\tau>0}\Phi_{Hn}|$, for all $n = 1, 2, \ldots, N$ (the term U is added to the definition of Φ_H in order to avoid dividing by zero). The new phase reveals similar results to those observed in the case for the phase Φ defined earlier. In fact, Fig. 4(a3) and (b3) show the constant and semi-periodic behaviour of Φ_H when heterogeneity in the parameters is identical to the two cases discussed in panels (a2) and (b2), respectively. The resemblance in behaviour between the two phases suggests that Φ_H could alternatively measure the level of synchrony in a population model equally well.

6. Averaged model

Investigating synchrony in system (15) and (16) is a very challenging task when heterogeneity appears in all parameters. The presence of $N + 1$ variables in this highly nonlinear system is what makes this task hard to tackle. Since most of the properties of the reduced one cell model have been analyzed in Section 4, it would be a good idea to reduce system (15) and (16) to a two-variable model through an averaging process. Such a step is motivated by the numerical results obtained in [21], demonstrating that a population of model neurons based on the four-variable model derived from system (1)–(6) exhibits parametric averaging and recruitment phenomena. Similar kind of parametric averaging behaviour has been also reported in [30–32]. We shall demonstrate in this section that reducing the population model by applying an averaging process is feasible when system (15) and (16) possesses heterogeneity in the parameter κ only, a case that has not been analyzed before. We intend to compare the dynamics of this system to a two-variable model whose κ value is the geometric average of all κ_n, $n = 1, 2, \ldots, N$, while all the other parameters remain identical in both models (such a two-variable model will be called the averaged model hereafter). In other words, we shall set the κ value of the averaged model to $\widetilde{\kappa} = \sqrt[N]{\kappa_1\kappa_2\ldots\kappa_N}$. The reason for choosing the geometric average over an algebraic average lies in the fact that the former performs better than the latter when comparing the behaviour of the population model to the averaged model (provided that all $\kappa_n, n = 1, 2, \ldots, N$, belong to the oscillatory domain of κ determined by the one cell model).

Fig. 5(a) and (b) show the temporal profiles of g for the population model consisting of 50 coupled model neurons and the averaged model, respectively. The parameters κ_n in the population model were chosen randomly from the range [610, 910] by using the uniform distribution as a random number generator, while $\widetilde{\kappa} \approx 752$ was chosen for the averaged model. Although the range-size of κ was 300, the two models produced comparable results (see Fig. 5(a) and (b)). In fact, the frequency and amplitude of g in both cases appear to be very similar. In order to thoroughly compare the two models given any parameter range of κ lying within the oscillatory domain, we use the notion of deviation measure, defined by

$$\text{Dev} = \frac{1}{T}\left[\int_0^T (g(\tau) - \widetilde{g}(\tau))^2 \mathrm{d}\tau\right]^{1/2}, \tag{18}$$

where g and $\widetilde{g}$ correspond to the population and averaged models, respectively. This new measure evaluates the difference in the average amount of g secreted by both models at steady state for a duration of length T. In the example shown in Fig. 5(a) and (b), the deviation of the averaged model from the population model between $\tau = 10^4$ and $\tau = 2 \times 10^4$ is given by Dev $\approx$ 11.478. This is equivalent to an average amount of 3.9 nM difference in the amount of GnRH secreted by both models during a time span of approximately 18.5 h which is very small relative to the average amount of GnRH secreted by both models separately.

Motivated by this example, we have evaluated the deviation measure for increasing ranges of κ centered around the value

Table 2
Values of the standard parameters of the model given by system (A.1)–(A.6). Parameters in roman style symbols are obtained by curve fitting to experimental data in [1].

Symbol	Value	Symbol	Value	Symbol	Value	Symbol	Value
J_{IN}	0.2 μM/min	b_G	0.144 nM/min	ℓ	60 min^{-1}	k_G	0.6 min^{-1}
k_A	60 min^{-1}	k_C	5100 min^{-1}	v_G	324 $(nM)^{-4}$ min^{-1}	v_C	1200 $(nM)^{-1}$ min^{-1}
C_{ER}	2.5 μM	b_A	1.8 nM/min	h_I	0.036 nM	K_S	0.34 nM
K_Q	21 nM	K_I	158 nM	k_S	9 min^{-1}	k_Q	9 min^{-1}
k_I	0.1125 min^{-1}	v_A	150 min^{-1}	v_S	23.4 nM/min	v_Q	22.5 nM/min
v_I	0.36 nM/min						

760. Fig. 5(c) shows that the deviation measure stays roughly at a low constant level and never exceeds 16 even when the range of κ is given by [60, 1460]. In other words, the averaged model represent a good approximation for the population model when the coupling between neurons is achieved by a shared signal. In Fig. 5(c), the geometric average $\widetilde{\kappa}$ has been plotted versus the length of the range of κ in the population model to reveal the values of $\widetilde{\kappa}$ used in the averaged model. This suggests that analyzing the $(N+1)$-dimensional population model directly is unnecessary as it behaves almost identical to a one cell model whose parameters satisfy certain averaging properties. In the case of the parameter κ, this averaging appears to be a geometric average.

It should be mentioned here that we have repeated the same analysis described above by using an algebraic average of κ instead of $\widetilde{\kappa}$. The values of the deviation measure in this case were considerably higher than those produced by the geometric average (results not shown). In other words, the outcome of the averaged model incorporating the geometric average outperformed the one incorporating the algebraic average. This was not the case, however, when the parameter range for κ used to generate heterogeneity in the population model, stretched far below the oscillatory domain of the one neuron model (a biologically unrealistic scenario). The geometric average, in this case, winded up lying outside the oscillatory domain while making the averaged model (expectedly) quiescent, although the population model remained pulsatile. The algebraic average, on the other hand, remained in the oscillatory domain in these cases, preserving the pulsatility of the averaged model but significantly altering it from the population model. In certain extreme cases when the parameter range for κ substantially exceeded the oscillatory domain, even the algebraic average ended up lying outside the oscillatory domain and forming a quiescent averaged model, while the population model remained pulsatile (results now shown). It seems that the nonlinearly of the functions F_n and H_n in Eqs. (15) and (16) is responsible for this peculiar behaviour.

7. Conclusion

We have investigated in this paper a recent model describing the dynamics of GnRH neurons. This model was first nondimensionalized and further reduced to a two-variable model to simplify the analysis. The nullclines of the reduced model were sketched and examined to understand the dynamics of the one cell model. Several theoretical results regarding the existence and stability of steady states and periodic solutions were also obtained. These results were very critical for understanding the general dynamics of the population model generated from coupling model neurons by a shared signal (common pool). Such a coupling technique is different from those normally discussed in the literature of coupled oscillators. The main difference between them lies in the fact that the common pool, g, here plays an indispensable role in generating oscillations in the population model. i.e., without g, the population model is quiescent and each member is nonoscillatory. In the classical studies of synchronization, however, removing the coupling terms between neurons in a population model has no impact on the ability of these individual neurons to intrinsically oscillate (even in the presence of mean field coupling). This fundamental difference makes the models discussed here very unique and interesting. Their performance towards synchronization, for example, was quite unusual in the way they responded to heterogeneity. In this paper, we successfully managed, under certain heterogeneity conditions, to reduce the population model to a two-variable model using parametric averaging process. Several synchronization results were obtained when heterogeneity was limited to certain parameters in the model, while for the general case of a diversely heterogeneous population, we introduced two different phases that provide some insight on how the model behaves under such conditions. Proving synchrony in this general case, however, remains an open question

Acknowledgements

This work was financially supported by MITACS (The Mathematics of Information Technology and Complex systems) grant to Professor L. Edelstein-Keshet. Discussion with Professor Y.X. Li (University of British Columbia) greatly benefited the general presentation of this manuscript.

Appendix A. Nondimensionalization of the original model

We aim in this section to nondimensionalize the GnRH model presented in [20]. The original six-variable model describing the dynamics of one neuron, is given by

$$\frac{dG}{dt} = b_G + v_G(AC)^3 - k_G G \tag{A.1}$$

$$\frac{dC}{dt} = J_{IN} + [\ell + v_C Q]\,(C_{ER} - C) - k_C C \tag{A.2}$$

$$\frac{dA}{dt} = b_A + v_A S \frac{h_I}{h_I + I} - k_A A \tag{A.3}$$

$$\frac{dS}{dt} = v_S \frac{G^4}{K_S^4 + G^4} - k_S S \tag{A.4}$$

$$\frac{dQ}{dt} = v_Q \frac{G^2}{K_Q^2 + G^2} - k_Q Q \tag{A.5}$$

$$\frac{dI}{dt} = v_I \frac{G^2}{K_I^2 + G^2} - k_I I, \tag{A.6}$$

where $K_S < K_Q < K_I$ represent the threshold levels of G for activating α_s, α_q and α_i, respectively. A detailed table containing all the parameters used in Eqs. (A.1)–(A.6) together with their values and units has been previously published in [20,21] and presented here in Table 2. To reduce the number of parameters used in system (A.1)–(A.6), we apply the following set of substitutions:

$$g = \frac{1}{K_S}G, \qquad c = \frac{v_C}{k_C}C, \qquad a = \frac{k_A}{b_A}A, \qquad s = \frac{k_S}{v_S}S$$

$$q = \frac{k_Q}{v_Q}Q, \qquad i = \frac{k_I}{v_I}I, \qquad \tau = k_S t.$$

This new set of scaled variables are dimensionless and satisfy Eq. (1)-(6), where

$$\lambda = \frac{k_G}{k_S}, \quad \nu = \frac{b_G}{k_G K_S}, \quad \eta = \frac{v_G}{k_G K_S}\left\{\frac{b_A k_C}{k_A v_C}\right\}^3, \quad \zeta = \frac{k_C}{k_S}$$
$$j_{in} = \frac{v_C J_{IN}}{k_C^2}, \quad \mu = \frac{\ell}{k_C}, \quad \delta = \frac{v_C v_Q}{k_C k_Q}, \quad c_0 = \frac{v_C C_{ER}}{k_C}$$
$$\xi = \frac{k_A}{k_S}, \quad \theta = \frac{v_A v_S}{b_A k_S}, \quad \omega = \frac{k_I h_I}{v_I}, \quad \psi = \frac{k_Q}{k_S}$$
$$\rho = \frac{K_Q}{K_S}, \quad \epsilon = \frac{k_I}{k_S}, \quad \kappa = \frac{K_I}{K_S}.$$

Appendix B. Behaviour of the fast subsystem

Here we demonstrate that the fast subsystem possesses only one globally stable equilibrium point by assuming that the slow variable g and i are roughly constants. Our main goal is to determine the global behaviour of the fast subsystem under these assumptions, and thus exclude the possibility that oscillations may occur in this subsystem.

By letting $g \approx p_1$ and $i \approx p_2$ (p_1 and p_2 are constants), the fast subsystem becomes

$$\frac{dc}{d\tau} = \zeta\left[j_{in} + [\mu + \delta q](c_0 - c) - c\right] \tag{B.1}$$
$$\frac{da}{d\tau} = \xi\left[\iota + \bar{\theta}s - a\right] \tag{B.2}$$
$$\frac{ds}{d\tau} = \phi\left[\bar{p}_1 - s\right] \tag{B.3}$$
$$\frac{dq}{d\tau} = \psi\left[\bar{p}_2 - q\right], \tag{B.4}$$

where $\bar{\theta} := \theta\omega/(\omega + p_2)$, $\bar{p}_1 := p_1^4/(\sigma^4 + p_1^4) < 1$ and $\bar{p}_2 := p_1^2/(\rho^2 + p_1^2) < 1$. Solving for the steady states of Eq. (B.1)-(B.4), we obtain only one equilibrium point, given by

$$c_{ss} = \frac{j_{in} + (\mu + \delta\bar{p}_2)c_0}{1 + \mu + \delta\bar{p}_2}, \quad a_{ss} = \iota + \bar{\theta}\bar{p}_1, \quad s_{ss} = \bar{p}_1, \quad q_{ss} = \bar{p}_2.$$

Notice that Eqs. (B.1)–(B.4) consist of two independent dynamic blocks; namely, $(s, a)^T$ and $(q, c)^T$, that are completely disjoint. By applying the substitution $x_1 = s - s_{ss}$, $x_2 = a - a_{ss}$, $y_1 = q - q_{ss}$ and $y_2 = c - c_{ss}$, the origin, $(0, 0)^T$, becomes the only equilibrium for the two dynamic blocks

$$\begin{cases} \dot{x}_1 = -\phi x_1 \\ \dot{x}_2 = \xi(\bar{\theta}x_1 - x_2) \end{cases} \tag{B.5}$$

and

$$\begin{cases} \dot{y}_1 = -\psi y_1 \\ \dot{y}_2 = \zeta(L_1 y_1 - \delta y_1 y_2 - L_2 y_2), \end{cases} \tag{B.6}$$

where $L_1 := \delta(c_0 - j_{in})/(1 + \mu + \delta\bar{p}_2)$ and $L_2 := 1 + \mu + \delta\bar{p}_2 > 1$.

The dynamic block (B.5) is linear with negative eigenvalues ($\lambda_1 = -\phi$ and $\lambda_2 = -\xi$). Thus, its equilibrium point $(0, 0)^T$ is globally stable. As for the nonlinear dynamic block (B.6), we need to apply the second Lyapunov method to establish that its own equilibrium $(0, 0)^T$ is also global stability. By choosing the Lyapunov function

$$V(y_1, y_2) = \frac{1}{2}\left(L_3 y_1^2 + \frac{1}{\zeta L_1} y_2^2\right) \geq 0,$$

for a given constant $L_3 > (L_1 + \delta)/2L_1\psi$, we obtain

$$\dot{V}(y_1, y_2) = -L_3\psi y_1^2 + y_1 y_2 - \frac{\delta}{L_1} y_1 y_2^2 - \frac{L_2}{L_1} y_2^2$$
$$\leq \left(\frac{1}{2} - L_3\psi + \frac{\delta}{2L_1}\right) y_1^2 + \left(\frac{1}{2} + \frac{\delta}{2L_1} y_2^2 - \frac{L_2}{L_1}\right) y_2^2.$$

Observe that $\frac{1}{2} - L_3\psi + \frac{\delta}{2L_1} < 0$, and that $\frac{1}{2} + \frac{\delta}{2L_1} y_2^2 - \frac{L_2}{L_1} < 0$, whenever $y_2^2 < (2L_2 - L_1)/\delta$ (where, according to Table 1, $(2L_2 - L_1)/\delta > 1$). This implies that $\dot{V}(y_1, y_2) < 0$, for all $(y_1, y_2)^T \in \{(y_1, y_2)^T \neq (0, 0)^T \mid y_2^2 \leq 1\}$. In other words, the equilibrium point $(0, 0)^T$ is stable in that set. Moreover, by applying the same technique used in the proof of Proposition 1, we could also show that $y_2 < 1$, for all $\tau > 0$. It follows that $(0, 0)^T$ is globally stable.

The above derivations demonstrate that the solution trajectories of the fast subsystem (B.1)–(B.4) eventually converge to their globally stable steady states. In other words, the variables of this subsystem do not exhibit any oscillatory behaviour and thus could hardly affect the general dynamics of the full model. This implies that the reduction step applied in Section 3 is valid.

References

[1] L.Z. Krsmanovic, N. Mores, C.E. Navarro, K.K. Arora, K.J. Catt, An agonist-induced switch in G protein coupling of the gonadotropin-releasing hormone receptor regulates pulsatile neuropeptide secretion, Proc. Natl. Acad. Sci. 100 (2003) 2969–2974.
[2] E. Knobil, On the control of gonadotropin in the rhesus monkey, Rec. Prog. Horm. Res. 36 (1980) 53–88.
[3] S.M. Moenter, R.M. Brand, A.R. Midgley, F.J. Karsch, Dynamics of gonadotropin-releasing hormone release during a pulse, Endocrinology 130 (1992) 503–510.
[4] M.J. Woller, E. Nicholas, T. Herdendorf, D. Tutton, Release of luteinizing hormone releasing hormone from enzymatically disperse rat hypothalamic explants is pulsatile, Biol. Reprod. 59 (1998) 587–590.
[5] E. Terasawa, Luteinizing hormone-releasing hormone (LHRH) neurons: Mechanism of pulsatile LHRH release, Vit. Horm. 63 (2001) 91–129.
[6] T.A. Richter, E. Terasawa, Neural mechanisms underlying the pubertal increase in LHRH release in the rhesus monkey, Trends Endocrinol. Metab. 12 (2001) 353–359.
[7] L.C. Krey, W.R. Butler, E. Knobil, Surgical disconnection of the medial basal hypothalamus and pituitary function in the rhesus monkey. I. Gonadotropin secretion, Endocrinology 96 (1975) 1073–1087.
[8] T.M. Plant, Y. Nakai, P. Belchetz, E. Keogh, E. Knobil, The sites of action of estradiol and phentolamine in the inhibition of the pulsatile circhoral discharges of LH in the rhesus monkey (Macaca mulatta), Endocrinology 102 (1978) 1015–1018.
[9] K.T. O'Byrne, J.C. Thalabard, P.M. Grosser, R.C. Wilson, C.L. Williams, M.D. Chen, D. Ladendorf, J. Hotchkiss, E. Knobil, Radiotelemetric monitoring of hypothalamic gonadotropin-releasing hormone pulse generator activity throughout the menstrual cycle of the rhesus monkey, Endocrinology 129 (1991) 1207–1214.
[10] M.J. Woller, S. Meyer, A. Ada-Nguema, D. Waechter-Brulla, Dissecting autocrine effects on pulsatile release of gonadotropin-releasing hormone in cultured rat hypothalamic tissue, Exp. Biol. Med. 229 (2003) 56–64.
[11] P.C. Goldsmith, R. Lamberts, L.R. Brezina, Gonadotropin-releasing hormone neurons and pathways in the primate hypothalamus and forebrain, in: R.L. Norman (Ed.), Aspects of Reproduction, Academic Press, New York, 1983, pp. 7–45.
[12] G. Martínez, de la Escalera, A.L.H. Choi, R.I. Weiner, Generation and synchronization of gonadotropin-releasing hormone (GnRH) pulses: Intrinsic properties of the GT1-1 GnRH neuronal cell line, Proc. Natl. Acad. Sci. 89 (1992) 1852–1855.
[13] E. Terasawa, K.L. Keen, K. Mogi, P. Claude, Pulsatile release of luteinizing hormone-releasing hormone (LHRH) in cultured LHRH neurons derived from the embryonic olfactory placode of the rhesus monkey, Endocrinology 140 (1999) 1432–1441.
[14] L.Z. Krsmanovic, A.J. Martinez-Fuentes, K.K. Arora, N. Mores, C.E. Navarro, H.C. Chen, S.S. Stojilković, K.J. Catt, Autocrine regulation of gonadotropin-releasing hormone secretion in cultured hypothalamic neurons, Endocrinology 140 (1999) 1423–1431.
[15] L.Z. Krsmanovic, S.S. Stojilković, L.M. Mertz, M. Tomic, K.J. Catt, Expression of gonadotropin-releasing hormone receptors and autocrine regulation of neuropeptide release in immortalized hypothalamic neurons, Proc. Natl. Acad. Sci. 90 (1993) 3908–3912.
[16] C. Xu, X.Z. Xu, C.S. Nunemaker, S.M. Moenter, Dose-dependent switch in response of gonadotropin-releasing hormone (GnRH) neurons to GnRH mediated through the type I GnRH receptor, Endocrinology 145 (2004) 728–735.
[17] M. Hyyppa, M. Motta, L. Martini, 'Ultrashort' feedback control of follicle-stimulating hormone-releasing factor secretion, Neuroendoc. 7 (1971) 227–235.

[18] L.V. Depaolo, R.A. King, A.J. Carrillo, In vivo and in vitro examination of an autoregulatory mechanism for luteinizing hormone releasing hormone, Endocrinology 120 (1987) 272–279.
[19] M.M. Valenca, C.A. Johnston, M. Ching, A. Negro-Villar, Evidence for a negative ultrashort loop feedback mechanism operating on the luteinizing hormone releasing hormone neuronal system, Endocrinology 121 (1987) 2256–2259.
[20] A. Khadra, Y.X. Li, A model for the pulsatile secretion of gonadotropin-releasing hormone from synchronized hypothalamic neurons, Biophys. J. 91 (2006) 74–83.
[21] Y.X. Li, A. Khadra, Robust synchrony and rhythmogenesis in endocrine neurons via autocrine regulations in vitro and in vivo, Bull. Math. Biol. 70 (2008) 2103–2125.
[22] Y. Kuramoto, Chemical Oscillations Waves and Turbulence, Springer-Verlag, Berlin, 1984.
[23] S.H. Strogatz, From kuramoto to crawford: Exploring the onset of synchronization in populations of coupled oscillators, Physica D 143 (2000) 1–20.
[24] A. Wagemakers, J.M. Buldú, J. García-Ojalvo, M.A.F. Sanjuán, Synchronization of electronic genetic networks, Chaos 16 (2006) 013127, 1–8.
[25] N. Kopell, G.B. Ermentrout, M.A. Whittington, R.D. Traub, Gamma rhythms and beta rhythms have different synchronization properties, Proc. Natl. Acad. Sci. 97 (2000) 1867–1872.
[26] Y.X. Li, Clustering in neural networks with heterogeneous and asymmetrical coupling strengths, Physica D 180 (2003) 210–234.
[27] A. Longtin, M. St-Hilaire, Encoding carrier amplitude modulations via stochastic phase synchronization, Int. J. Bifurcation Chaos 10 (2000) 1–16.
[28] M.G. Rosenblum, A.S. Pikovsky, J. Kurths, Phase synchronization of chaotic oscillators, Phys. Rev. Lett. 76 (1996) 1804–1807.
[29] J.N. Pandey, The Hilbert Transform of Schwartz Distributions and Applications, John Wiley & Sons, New York, 1996.
[30] Y.X. Li, J. Halloy, J.L. Martiel, A. Goldbeter, Suppression of chaos and other dynamical transitions induced by intercellular coupling in a model for cyclic AMP signaling in dictyostelium cells, Chaos 2 (1992) 501–512.
[31] Y. Manor, J. Rinzel, I. Segev, Y. Yarom, Low amplitude oscillations in the inferior olive: A model based on electrical coupling of neurons with heterogeneous channel density, J. Neurophys. 77 (1997) 2736–2752.
[32] J.H.E. Cartwright, Emergent global oscillations in heterogeneous excitable media: The example of pancreatic β cells, Phys. Rev. E 62 (2000) 1149–1154.